

Calculation of relative seismic attenuation from the reflection time-frequency differences in a carbonate reservoir

Han-ming Gu and Robert R. Stewart

ABSTRACT

Frequency characteristics of seismic reflections returning from reservoirs with fractures and voids are different from those of surrounding rock. These characteristics can be depicted by time-frequency analysis technology. The S-transform is applied to the time-frequency analysis of seismic reflections of reservoirs of carbonate rock with fractures and voids. Moreover, carbonate rock with fractures and voids filled with oil and gas can attenuate the amplitude of seismic waves. We present a method using the differences in seismic reflection time-frequency spectra to estimate relative seismic attenuation in a reservoir of carbonate rock with fractures and voids.

INTRODUCTION

In reservoirs with fractures and voids, one of the primary reservoir types in the Tahe oil field and its peripheral area, frequency characteristics of seismic reflections are different from those of the surrounding rock. The characteristics can be analyzed using time-frequency analysis technology. The earliest time-frequency analysis was implemented by the method of a short time window Fourier transform (Gabor, 1946; Portnoff, 1980). However, this method can only be used in the single resolution analysis method. A wavelet transform, applied to time-frequency in the late nineteen eighties (Wilson, et al, 1992; Satish, et al, 2003), overcomes the deficiency of single resolution in the short time window Fourier transform. The scale factor used in the wavelet transform is not directly related to frequencies. Therefore, wavelet transforms cannot be used to obtain true time-frequency spectra. Stockwell presented a method called S-transform time-frequency analysis in 1996 (Stockwell, 1996). This method overcomes the deficiencies in the short time window Fourier transform and in the wavelet transform. Later, some scholars presented several generalized S-transforms (McFadden et al., 1999; Pinnegar, et al, 2003; Gao et al., 2003), widening the applicability of S-transforms. We apply S-transforms to the time-frequency analysis of seismic reflections of reservoirs of carbonate rock with fractures and voids.

Carbonate rock with fractures and voids filled with oil and gas can attenuate the amplitude of seismic waves. Seismic attenuation is related to the liquid's properties in the reservoir (Best et al., 1994), and can be determined from the amplitude change of the seismic wave (Parker, 1994; Hauge, 1981). Given incident amplitudes and frequency spectra, seismic attenuation can be calculated by the conventional amplitude ratio method and frequency spectra ratio method. However, the reservoir thickness of carbonate rock with fractures and voids is, in general, less than a quarter of the seismic wavelength. Therefore, it is difficult to determine the seismic reflections at the top and bottom of the reservoir, required by the conventional method of calculating seismic attenuation. A method is presented, using the difference of seismic reflection time-frequency, to estimate relative seismic attenuation in such reservoirs.

SEISMIC TIME-FREQUENCY ANALYSIS BY THE S-TRANSFORM

Seismic reflection signals are non-stationary signals. Only joint time-frequency expressions, methods mapping a 1-D time-varying signal to a 2-D time-frequency plane, can analyze time-varying frequency signals. Time-frequency analytical methods may be linear or nonlinear. Typical linear time-frequency methods are the short time window Fourier transform, the wavelet transform, the S-transform, etc. Nonlinear time-frequency methods include the Cohen distribution, the Wigner-Ville distribution, etc.

The short time window Fourier transform (SWFT) time-frequency method allows one to acquire different frequency spectra at different time. The spectra are obtained from a time-varying signal by applying multiple time-varying short time window functions, which are Fourier transformed. As a short time window function corresponds to single time-frequency resolution, SWFT can only be used in single resolution analysis.

The wavelet transform (WT) time-frequency analytical method uses the indirect relationship between the scale used in WT and frequency to acquire time-varying frequency spectra. A large scale WT captures low frequencies of a signal, while a small scale WT represents high frequencies of a signal. In summary, WT time-frequency analysis is a multi-resolution method. However, the scale in the wavelet transform is not directly related to frequency, hence true time-frequency spectra cannot be obtained from wavelet transform.

In 1996, Stockwell presented S-transform time-frequency analysis. This method overcomes the shortages in short time-window Fourier transform and wavelet transform. The 1-D continuous forward S-transform can be expressed by (Stockwell, 1996)

$$S(\tau, f) = \int_{-\infty}^{\infty} h(t) \frac{|f|}{\sqrt{2\pi}} \times e^{\left[\frac{-f^2(\tau-t)^2}{2} \right]} e^{-2\pi i f t} dt \quad (1)$$

where $S(\tau, f)$ is the S-transform of signal $h(t)$; f is the frequency; t is time; τ is the central time of the Gaussian time-window function. Let a signal have N samples separated by sample interval Δ . Then the 1-D discrete forward S-transform can be expressed by

$$S\left[j\Delta, \frac{n}{N\Delta}\right] = \sum_{m=0}^{N-1} H\left[\frac{m+n}{N\Delta}\right] e^{-\frac{2\pi^2 m^2}{n^2}} e^{\frac{i2\pi m j}{N}} \quad (2)$$

The reciprocal of frequency determines the scale of the Gaussian time window in the S-transform. Hence, ST time-frequency analysis is a multi-resolution method. Therefore, the S-transform contains phase factors which preserve the phase character of each frequency.

COMPARISON OF THE ST AND SWFT TIME-FREQUENCY ANALYSIS METHODS

We use several time-window lengths, including 1/4, 1/2, 1, 2, 3 and 4 times the period of the wavelet to perform SWFT time-frequency analysis on a 30Hz Ricker wavelet, and to acquire time-frequency spectra as shown in Figures 1(b)-(g). The figures below show the

fact that, while time-window length grows, the resolution in the frequency domain increases, and the resolution in the time domain decreases. As a result, when time-frequency spectra are analyzed, it is necessary to choose a proper time window length. If the time window length is too short, false high frequency results will be incurred, if it is too long, there will be too much frequency overlap. From the figures, the resolution in the time domain and the frequency domain is compromised when the time window length equals the period of the wavelet.

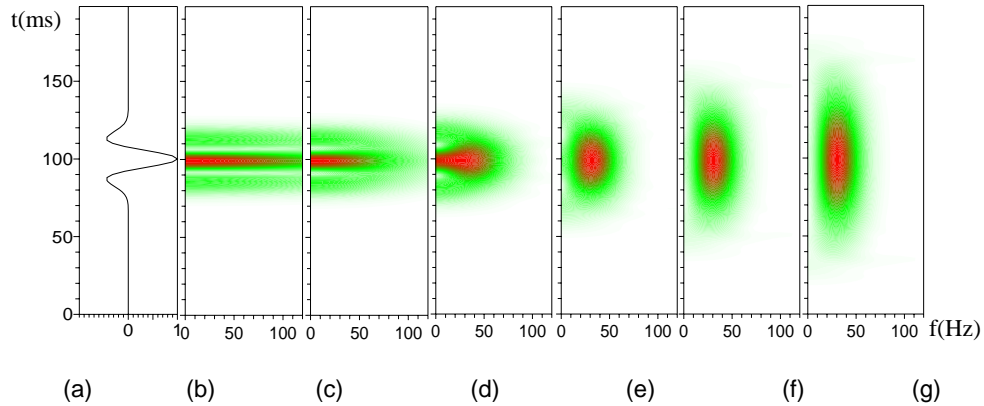


FIG. 1. SWFT time-frequency analysis with several time-window lengths.

Similarly, we also use several transform coefficients, ranging from 0.05, 0.08, 0.1, 0.5 to 1.0; to perform ST time-frequency analysis of the Ricker wavelet above; and to acquire the time-frequency spectra shown in Figures 2(b)-(g). From these figures, note the fact that while the transform coefficient grows, the resolution in the frequency domain increases, and the resolution in time domain decreases. This method also requires a proper transform coefficient.

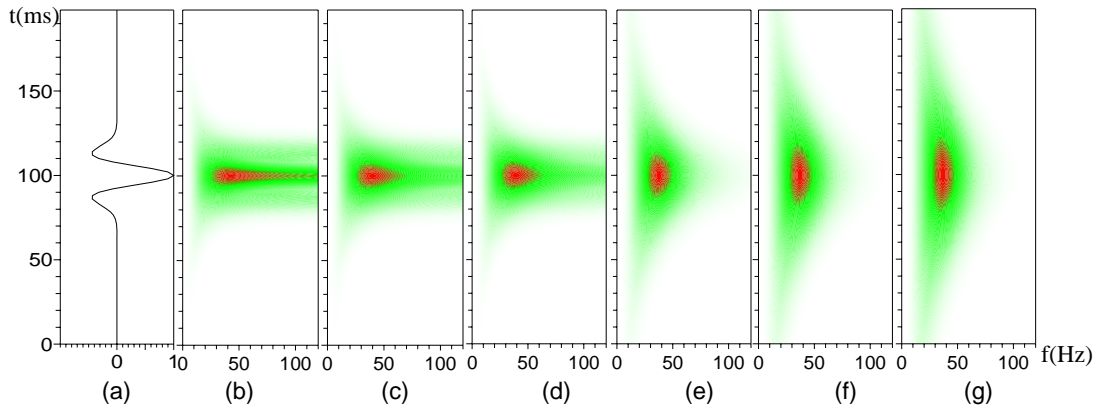


FIG. 2. ST time-frequency analysis with several transform coefficients.

Figures 3(b) and (c) show respectively the results of SWFT and ST time-frequency analysis of the trace synthetic seismogram shown in Figure 3(a). The dominant frequency of the wavelet increases with time, 30Hz, 40Hz, 50Hz, and 60 Hz for the events in the ranges shown in Figure (3b). The time window length is a constant 33 ms in the SWFT and the transform coefficient is a constant 0.1 in the ST. These figures show that the resolution in the frequency domain goes down when the dominant frequency goes up. Hence, the time window length or transform coefficient should be separately chosen

when time-frequency analysis is applied to different time segments of seismic data. Figures 4(b) and (c) show respectively the results of SWFT and ST time-frequency analysis of a trace seismogram at well TK610 in the Tahe oil field area shown in Figure 4(a). It shows the resolution in the frequency domain to vary with time.

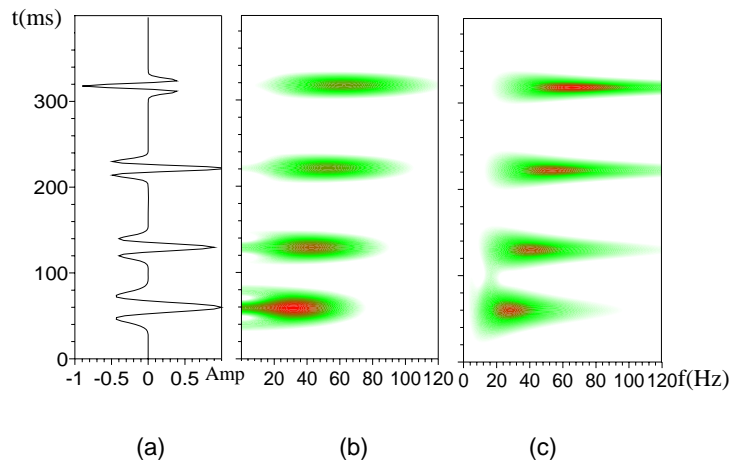


FIG. 3. Time-frequency analysis of a trace synthetic seismogram. (a) Seismogram; (b) time-frequency analysis by SWFT; (c) time-frequency analysis by ST.

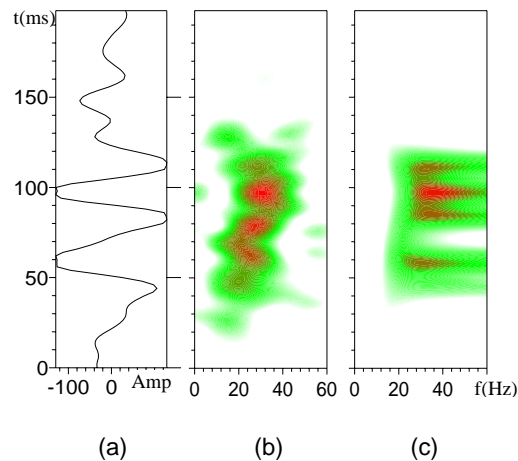


FIG. 4. Time-frequency analysis of a seismogram at well TK610. (a) Seismogram; (b) time-frequency analysis by SWFT; (c) time-frequency analysis by ST.

From the result of comparison of above Figures, the resolution in frequency domain and in time domain from ST is higher than that from SWFT.

TIME-FREQUENCY ANALYSIS OF SYNTHETIC AND FIELD SEISMOGRAMS

Time-frequency analysis of synthetic seismograms

In order to analyze the time-frequency characteristics of seismic responses from rocks with voids of different heights, width and filling, this investigation is based on the developed features of the carbonate rock in the Tahe area, modeled by designing 9 types of voids. Synthetic common-shot-point seismograms were computed using modeling software developed by Tesserall Co., Canada, according to the field layout. The dominant

frequency Ricker wavelet is 25 Hz. Then, Focus software was used to perform velocity analysis and post-stack migration shown in Figure 5.

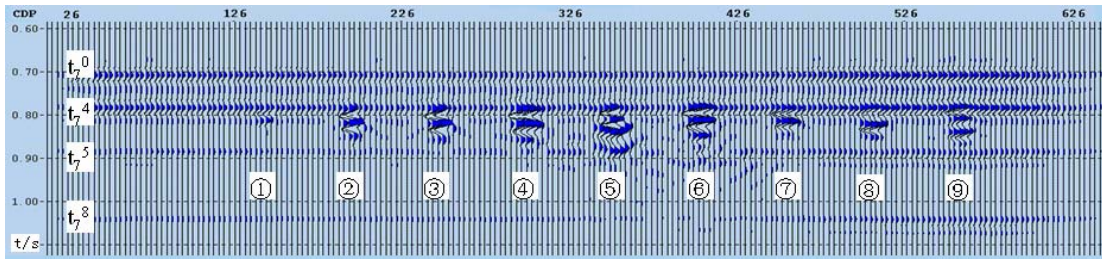


FIG. 5. Post-stack migration result of synthetic shot records. The height of all voids is 10 m. Void widths 1-4 are 10 m, 20 m, 40 m, 80 m respectively. Void 5 is made up of two voids whose width are 40 m and 80 m with a vertical separation of 10 m. Void 6 is made up of three voids with a vertical separation of 10 m, whose width are 20 m, 40 m and 80 m. Voids 7-9 are respectively the same as Voids 1-4. Void 1-6 are full of oil and gas. Void 7-9 are compactly filled.

Figure 6 shows time-frequency analyses of a trace seismogram of voids 1, 2 and 5. It can be seen that the time-frequency features of voids 1 and 2 under the T_7^4 event are similar, but the time-frequency spectrum of void 5 has two extrema under the T_7^4 event. This is because of the two overlapped voids. Therefore, time-frequency features can be used for the ability to resolve lithologic voids in seismic records.

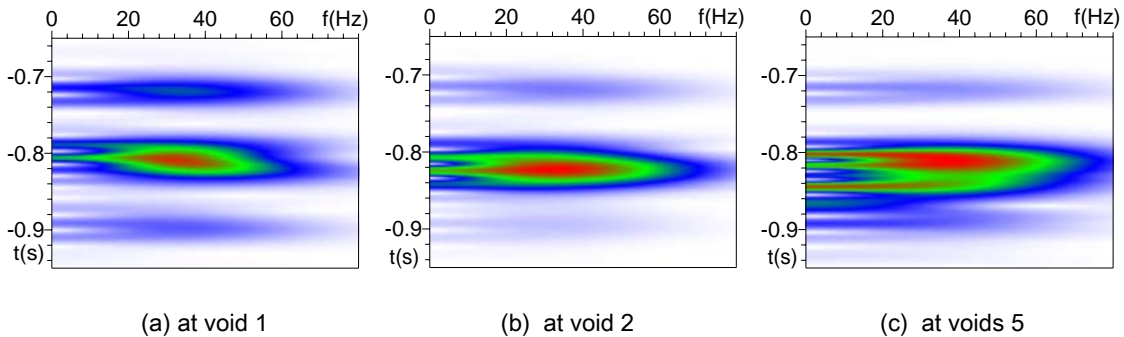


FIG. 6. Time-frequency analysis of trace seismograms over the voids of Figure 5.

Figure 7 is a time-frequency analysis of seismograms along the T_7^4 event. The red and green colors symbolize the steep changes of time-frequency spectra energy. These figures show that these areas correspond to horizontal positions of voids. In particular, the reflective amplitude of void 1 is very weak in the seismic record, but the void can be clearly seen in time-frequency spectra.

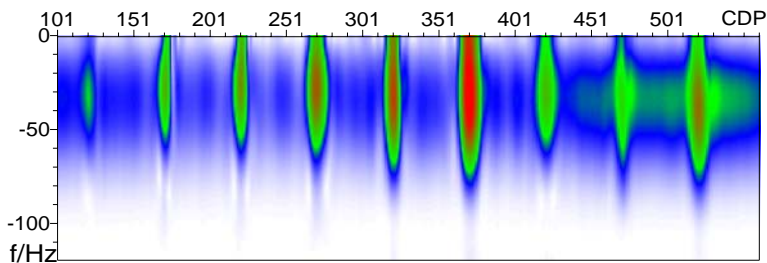


FIG. 7. Time-frequency analysis of a seismogram along the T_7^4 event of Figure 5.

Figure 8 shows time-frequency spectra at 15 Hz and at 38 Hz of the synthetic seismograms of Figure 5. The red and green colors indicate rapid and steep changes of time-frequency spectra energy and anomalous spectra. The locations of anomalous spectra can pinpoint the locations of developed voids well. The black curve outlines the maximum spectrum of each trace. It also shows that the horizontal locations of the spectral maxima correspond to locations of developed voids. Spectral energy at 15 Hz has stronger amplitude than that at 38 Hz. In this figure it is difficult to distinguish different seismic responses due to different void filling.

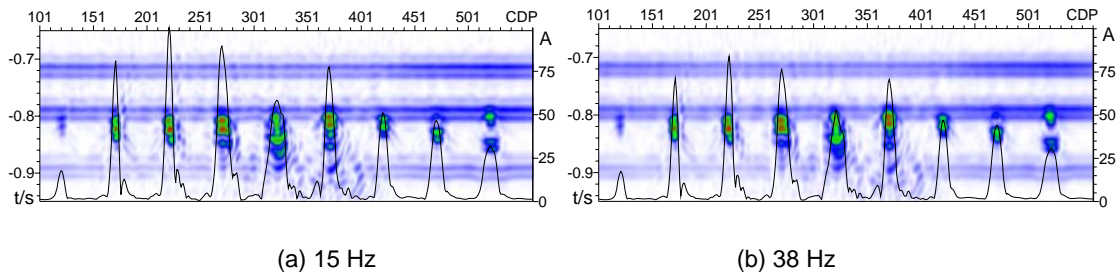


FIG. 8. Time-frequency spectra, at two frequencies, of synthetic seismograms of Figure 5.

Time-frequency analysis of field seismic records

The field area is located at the southern Tahe oil field. There are 6 wells in the area. The reservoir at TK610 (Line: 2589, Time: 35ms) has well developed fractures full of oil and gas under layer T_7^4 ; the reservoir at T601 (Line: 2625, Time: 20ms) has well developed voids full of oil under layer T_7^4 ; The reservoir at TK735 has well developed fractures and voids full of water; the reservoir at TK620 has well developed fractures.

Figure 9 is an in-line time-frequency analysis across TK610 and T601 under event T_7^4 at 0 ms, 10, 20, and 30 ms. Seismic v_{CDP} e frequencies varied from time to time. f_{CDP} e 10 shows 15, 30, 45, 60 Hz time-frequency horizontal slices under layer T_7^4 for a 0-20 ms time window. Compared with the condition of reservoirs at wells in the area, low frequency spectrum is related to well reservoirs with fractures and voids.

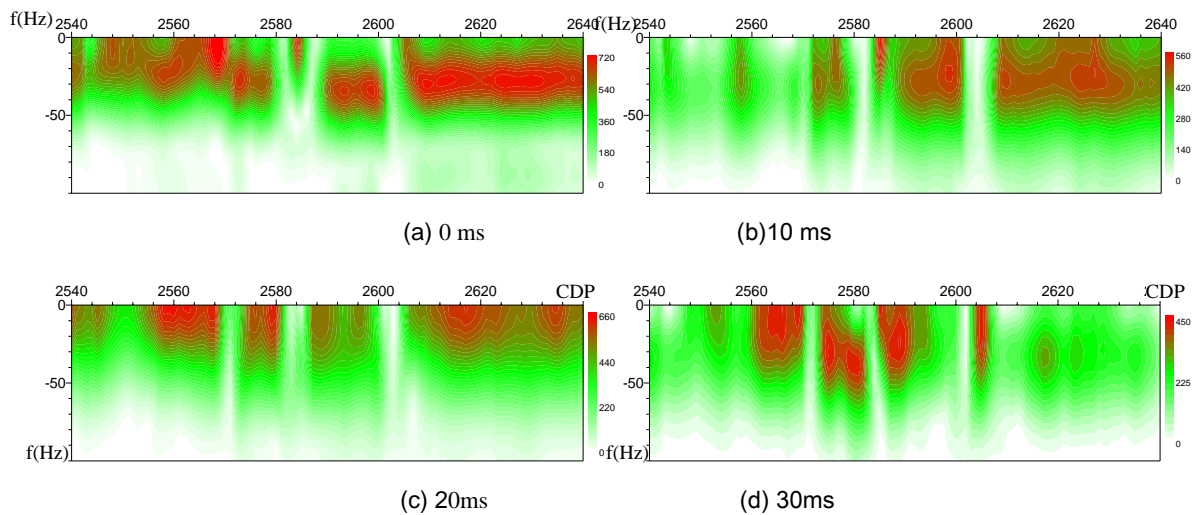


FIG. 9. The layer-following time-frequency analysis across TK610 and T601 under event T_7^4 different time.

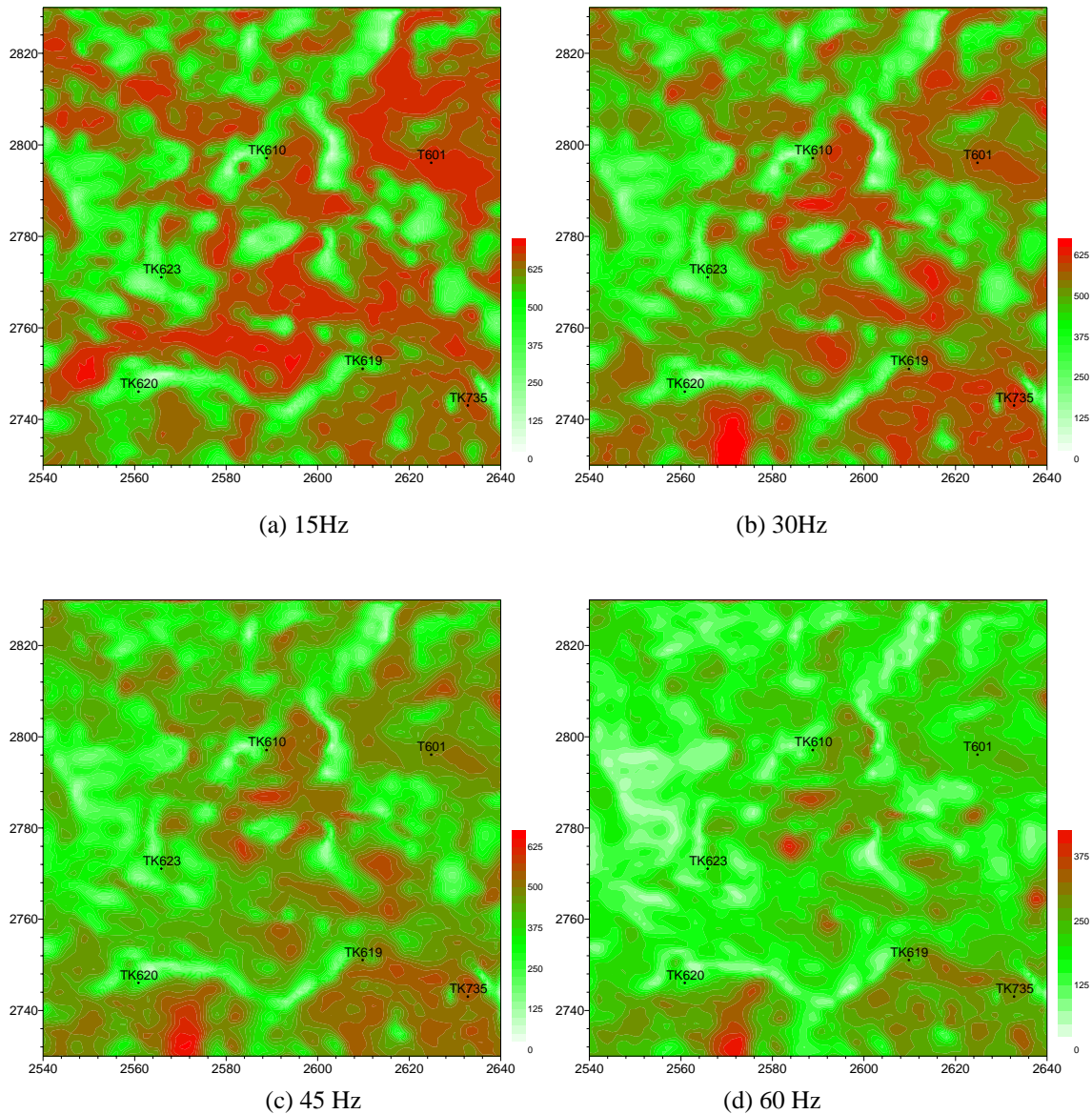


FIG. 10. Time-frequency horizontal slices corresponding to several frequencies under layer T_7^4 for a 0-20 ms time window.

THE METHOD CALCULATED ATTENUATION BY TIME-FREQUENCY SPECTRA DIFFERENCES

Wave propagation and absorption in a medium

Let the amplitude spectrum of an incident wave be $S(f)$, with a medium response $G(f)H(f)$, then the reflection amplitude spectra $R(f)$ may be expressed (Youli and Jerry, 1997) as

$$R(f) = G(f)H(f)S(f) \quad (3)$$

where the factor $G(f)$ includes geometric spreading, instrument response, source and receiver coupling, and reflection and transmission coefficients, and the phase

accumulation caused by propagation. The factor G may be taken to be independent of frequency. $H(f)$ describes the attenuation effect on the amplitude. Attenuation is usually proportional to frequency, and the response $H(f)$ may be expressed (Ward and Toksoz, 1971) as

$$H(f) = \exp\left(-f \int_l \alpha_0 dl\right), \quad (4)$$

where the integral is taken along the raypath, and α_0 is the attenuation coefficient.

Analytical expression of the differences of reflection spectra corresponding to two frequencies and an attenuation coefficient

First, let us consider a special case where the incident spectrum $S(f)$ has a Gaussian distribution, and discuss the reflection centroid frequency downshift. Then, we give the analytical expression of the differences of reflection spectra corresponding to the two frequencies with an attenuation coefficient. Last, we show that the differences of reflection spectra corresponding to the two frequencies which are symmetrical to the centroid frequency and separated by twice the incident signal's standard deviation may be used to calculate attenuation the coefficient.

If the source amplitude spectrum is Gaussian, the received amplitude spectrum may be expressed (Youli and Jerry, 1997) as

$$S(f) = \exp\left[-\frac{(f - f_s)^2}{2\sigma_s^2}\right], \quad (5)$$

$$R(f) = A \exp\left[-\frac{(f - f_R)^2}{2\sigma_s^2}\right], \quad (6)$$

$$f_R = f_s - \sigma_s^2 \int_l \alpha_0 dl, \quad (7)$$

$$f_d = 2f_s \sigma_s^2 \int_l \alpha_0 dl - \left(\sigma_s^2 \int_l \alpha_0 dl\right)^2, \quad (8)$$

$$A = G \exp\left[-\frac{f_d}{2\sigma_s^2}\right], \quad (9)$$

where f_s and σ_s^2 are respectively the centroid frequency and the variance of the incident amplitude spectrum. f_R is the centroid frequency of the reflected amplitude spectrum. Equation (7) shows that the reflection centroid frequency is downshifted toward lower frequencies.

If the differences between the reflection spectra corresponding to the two frequencies are related to the attenuation coefficient, the equation (5) shows that the incident

spectrum does not include the spectral changes caused by the absorption coefficient. Therefore, the difference between the incident spectra corresponding to the two frequencies must be zero, and only the differences of incident spectra corresponding to the two frequencies symmetrical to the incident centroid frequency could be zero. Hence, the differences between reflection spectra corresponding to the two frequencies symmetrical to the incident centroid frequency can include the changes in the reflection spectrum caused by the absorption coefficient.

Let Δf be the difference between a frequency and the centroid frequency of the incident spectrum. In the following, this paper is going to prove the fact that the difference of reflected spectra at $f_s - \Delta f$ and $f_s + \Delta f$ is related to absorption attenuation and must have an optimum Δf , which makes the difference a maximum. This difference can also yield a good measure for the absorption attenuation.

From equation (6), the difference $\Delta R(\Delta f)$ can be expressed as

$$\begin{aligned} \Delta R(\Delta f) &= R(f_s - \Delta f) - R(f_s + \Delta f) \\ &= A \exp\left[-\frac{(f_s - \Delta f - f_R)^2}{2\sigma_s^2}\right] - A \exp\left[-\frac{(f_s + \Delta f - f_R)^2}{2\sigma_s^2}\right] \end{aligned} \quad (10)$$

Let the distance of reflection wave propagation be L . If the absorption attenuation within the distance is constant, equation (9) can be rewritten as

$$f_R = f_s - \sigma_s^2 L \alpha_0. \quad (11)$$

From equations (10) and (11) we can write $\Delta R(\Delta f)$ as

$$\Delta R(\Delta f) = A \exp\left[-\frac{(\alpha_0 L \sigma_s^2 - \Delta f)^2}{2\sigma_s^2}\right] [1 - \exp(-2L\alpha_0\Delta f)]. \quad (12)$$

As absorption attenuation α_0 usually is of the order of magnitude of 10^{-5} , and the thickness of the target layer such as the carbonate rock with fractures and voids is small, compared relative to Δf , $\sigma_s^2 L \alpha_0$ can be ignored and $2L\alpha_0\Delta f \ll 1$, then equation (12) can be simplified to

$$\Delta R(\Delta f) \approx 2AL\alpha_0\Delta f \exp\left[-\frac{\Delta f^2}{2\sigma_s^2}\right] \quad (13)$$

When the high power of α_0 is ignored, equation (8) can be simplified to

$$f_d = 2f_s\sigma_s^2L\alpha_0 \quad (14)$$

Putting equation (14) into equation (9), we can obtain

$$A = G \exp(-f_s L \alpha_0) \approx G(1 - f_s L \alpha_0) \quad (15)$$

Putting equation (15) into equation (13) and ignoring the high power of α_0 , we can obtain

$$\Delta R(\Delta f) \approx 2GL\Delta f \alpha_0 \exp\left[-\frac{\Delta f^2}{2\sigma_s^2}\right] \quad (16)$$

and,

$$\alpha_0 \approx \frac{\Delta R(\Delta f)}{2GL\Delta f} \exp\left(\frac{\Delta f^2}{2\sigma_s^2}\right) \quad (17)$$

Equation (17) shows that the differences of reflection spectra corresponding to the two frequencies symmetrical to the incident centroid frequency can be used to calculate the absorption coefficient.

Equation (17) is used to calculate absorption attenuation, it must have an optimal Δf which makes the difference of reflected spectra at $f_s - \Delta f$ and $f_s + \Delta f$ a maximum. Hence there is a Δf that makes the derivative of equation (11) with respect to Δf zero, i.e.

$$\frac{\partial}{\partial \Delta f} [\Delta R(\Delta f)] = \frac{\partial}{\partial \Delta f} \left\{ A \exp\left[-\frac{(\alpha_0 L \sigma_s^2 - \Delta f)^2}{2\sigma_s^2}\right] [1 - \exp(-2L\alpha_0 \Delta f)] \right\} = 0$$

Then,

$$[1 - \exp(-2\alpha_0 L \Delta f)] \left(\alpha_0 L - \frac{\Delta f}{\sigma_s^2}\right) + 2\alpha_0 L \exp(-2\alpha_0 L \Delta f) = 0 \quad (18)$$

Using $2L\alpha_0 \Delta f \ll 1$ simplifies the above equation to

$$\Delta f^2 + \alpha_0 L \sigma_s^2 \Delta f - \sigma_s^2 = 0$$

Then,

$$\Delta f = -\alpha_0 L \sigma_s^2 / 2 + \sigma_s \sqrt{1 + L^2 \alpha_0^2 / 4} \approx \sigma_s \quad (19)$$

From Equation (17) and (19) follows that the differences of reflection spectra corresponding to the two frequencies which are symmetrical to the centroid frequency and separated by twice the incident wave's standard deviation yield a maximum.

Putting equation (19) into equation (17), we obtain

$$\alpha_0 \approx \frac{R(f_s - \sigma_s) - R(f_s + \sigma_s)}{2GL\sigma_s \exp(-0.5)} \quad (20)$$

In the area of a target layer such as reservoirs of carbonate rocks with fractures and voids, the thickness of the reservoir usually varies little laterally, and the denominator of expression (20) can be taken to be constant. Therefore, the differences between the

reflection spectra corresponding to the two frequencies can truly express the relative size of absorption attenuation.

What has been discussed above refers to an incident amplitude spectrum of Gaussian shape. The incident wave is often taken as a Ricker wavelet, and zero or minimum phase deconvolution is usually applied to field seismic records in seismic data processing. Therefore, the seismic wavelet is similar to the Ricker wavelet. Table 1 shows the dominant frequency of the Ricker wavelet and the centroid frequency, and the standard deviation from fitting a Gaussian to the amplitude spectrum of the Ricker wavelet. As a result, the centroid frequency is close to the dominant frequency of the Ricker wavelet, which shows that the amplitude spectrum shape is close to Gaussian in shape. Hence, what has been discussed above can be extended without any substantial loss of generality.

Table 1. The dominant frequency of the Ricker wavelet and the centroid frequency and standard deviation from using Gaussian shape fitting the amplitude spectrum of the Ricker wavelet.

No.	dominant frequency (Hz)	centroid frequency (Hz)	Standard deviation (Hz)
a	25	26.2	11.7
b	30	31.2	14.3
c	35	36.5	16.5
d	40	41.7	19.1

THE CALCULATION OF ABSORPTION ATTENUATION FROM SYNTHETIC AND FIELD SEISMOGRAMS

The lateral difference variation of reflected time-frequency spectra presents the lateral relative absorption attenuation variation in absorptive media. Moreover, strong absorption attenuation is closely related to the carbonate rock reservoir with developed fractures and voids full of oil and gas. Hence, this paper applies ST time-frequency analysis mentioned above to calculate spectral attributes at each time and predict reservoirs with fractures and voids using the difference of reflection time-frequency spectra.

The calculation of absorption attenuation from synthetic seismograms

The dominant frequency of a wavelet in the synthetic seismograms shown in Figure 5 is 25 Hz. From table 1 follows that the centroid frequency and standard deviation obtained by fitting Gaussians on the amplitude spectrum of the Ricker wavelet are respectively 26.2 Hz and 11.7 Hz. As a result, the differences of reflected spectra corresponding to the two frequencies which separately equal to 15 Hz and 38 Hz can present the size of relative absorption attenuation in the media (shown in Figure 11).

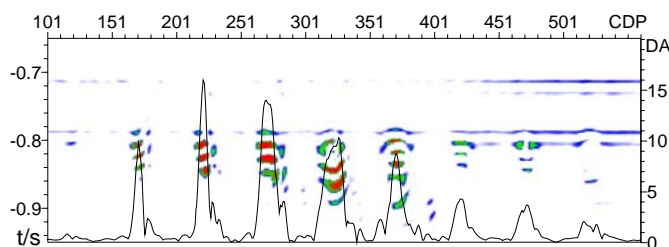


FIG. 11. The difference of reflected spectra corresponding to 15 and 38 Hz from synthetic seismograms.

The red and green colors symbolize the high values of the relative absorption attenuation. Compared to the model designed, the anomalies of relative absorption attenuation correspond to the position of voids except for No.1. The bold black curve in Figure 11 expresses maximum relative absorption attenuation within a time-window at each CDP. The sizes of relative absorption attenuation at voids 2-6 are very close. The sizes of the relative absorption attenuation at voids 7-9 are also very close but the sizes of the relative attenuation coefficients at voids 2-6 are evidently larger than that at voids 7-9. The reason is that the fillings in voids 2-6 are fluid while voids 7-9 contain lightly compacted materials.

Calculation of absorption attenuation from field seismic records

The reservoirs are primarily developed under event T_7^4 0-60 ms in the area. The event T_7^4 can be taken as the incident wave of the reflection of the reservoirs. From spectral analysis, we obtained values at 32.2 Hz and 11.4 Hz respectively for the centroid frequency and standard deviation from using Gaussians fitted to the amplitude spectrum of event T_7^4 . As a result, the difference of reflection spectra corresponding to the two frequencies of 21 Hz and 44 Hz yields the size of relative absorption in the media. Figure 12 shows that the differences of reflection spectra correspond to the two frequencies from ST time-frequency analysis to field seismic data across TK610 and T601 under event T_7^4 for a window of 0-80 ms. Red colors indicate the high values of relative absorption attenuation. From equation (20), the anomalies of relative absorption indicate the well developed reservoirs. The anomalies of relative absorption appear within about 35-40ms under the T_7^4 layer at well TK610 (Line 2589) and about 15-20ms under layer T_7^4 at well T601 (Line 2625), and the anomalies of relative absorption at well TK610, are very high. These anomalies are closely related to the properties of reservoirs developed at the wells.

Figure 13(a) shows a horizontal slice of differences of reflection amplitude spectra corresponding to the two frequencies 21 Hz and 44 Hz under event T_7^4 within the time window 0-20ms. The red colors represent large relative magnitudes or large anomalies of absorption. Compared to the growth of reservoirs and their filling, the large absorption anomaly at well T601 corresponds to the void filled with oil. Slightly larger absorption anomalies at well TK619 and TK735 correspond to the fractures and voids filled with oil. It should be noted that there is a large absorption anomaly between well TK620 and TK623; however, since there is no obvious high value in the time-frequency spectrum in Figure 10, it can be deduced that this area corresponds to the growth of fractures.

Figure 13(b) shows a horizontal slice of differences of reflection amplitude spectra corresponding to the two frequencies of 21 Hz and 44 Hz under the event T_7^4 , within the time window of 20-40ms. Compared to the 6 wells penetrating reservoirs with growth or filling in them, the high abnormality of absorption attenuation at well TK610 corresponds to growth fractures full of oil. Hence, it can be deduced that the anomalies of relative absorption between well TK620 and TK619 correspond to the growth of fractures and voids.

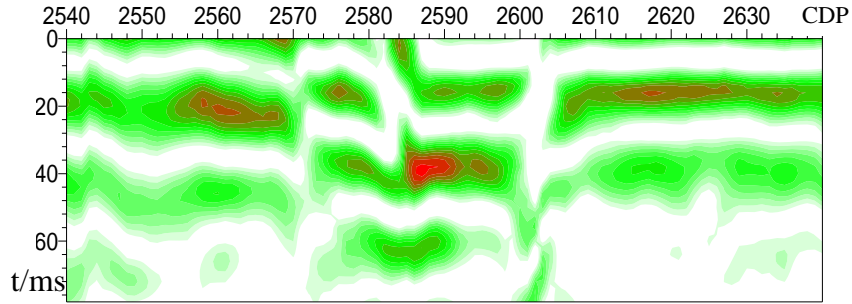


FIG. 12. The difference of reflection spectra corresponding to 21 and 44 Hz from field seismograms.

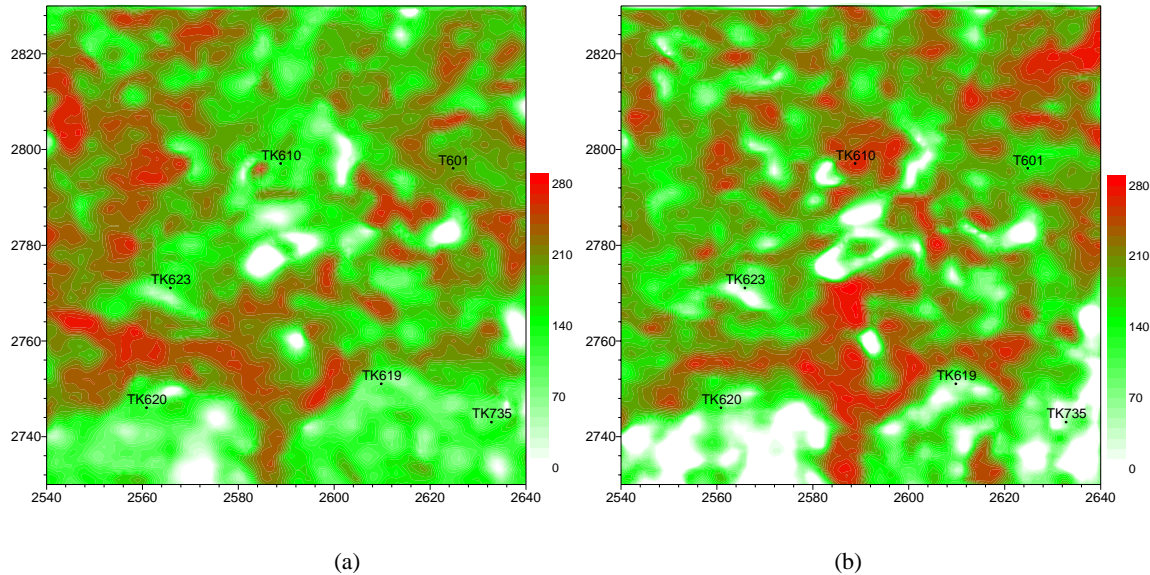


FIG. 13. Horizontal slices of differences of reflection amplitude spectra corresponding to the two frequencies 21Hz and 44Hz under event T_7^4 , within a time window. (a) 0-20 ms; (b) 20-40 ms.

CONCLUSIONS

(1) The time-frequency features of synthetic and field seismograms show that the attributes from ST time-frequency analysis can quantitatively recognize the anomaly of amplitude and frequency of seismic reflections from reservoirs with fractures and voids filled with oil or gas.

(2) The difference between reflection amplitude spectra corresponding to two frequencies symmetrical to the incident centroid frequency relates to the relative absorption attenuation.

(3) The difference between reflection spectra corresponding to the two frequencies which are symmetrical to the incident centroid frequency and separated by twice the incident wave's standard deviation can be used to calculate the attenuation coefficient.

(4) The difference of amplitude spectra corresponding to the two frequencies of 21 Hz and 44 Hz under the event T_7^4 within the time window from 0-20 ms and from 20-40 ms in the Tahe oil field area provides a measure for the relative absorption attenuation in reservoirs with fractures and voids.

ACKNOWLEDGEMENTS

We greatly appreciate Bianca Geng for her excellent suggestions and editing of this paper. We would like to thank Rolf Maier and David Henley for their reviews of this paper, and Hanxin Lu and Chuck Ursenbach for their constructive and thoughtful reviews, and we thank Kevin Hall for his assistance with in computing. We would also like to thank the CREWES sponsors for their support of this research. This research is also funded by the Northwest Petroleum Bureau, SINOPEC, of China.

REFERENCES

- Best, A. I., McCann, C., and Sothcott, J., 1994, The relationships between the velocities, attenuations, and petrophysical properties of reservoir sedimentary rocks: *Geophys. Prosp.*, **42**, 151-178.
- Gabor, G., 1949, Thoery of communication: *Journal of the IEEE*. 429-497.
- Gao X.W., Chen W.C., and Li Y.M., 2003, Generalized S-transform and the analysis of seismic response in thinlayer: *Acta Geophysica Sinica*, **46**, 526-532.
- Hauge, P., 1981, Measurements of attenuation from vertical seismic profiles: *Geophysics*, **46**, 1548-1558.
- McFadden, P.D., Cook, J.G., and Forster, L.M., 1999, Decomposition of gear vibration signals by the generalized S-transform: *Syst. Signal Process*, **13**, 691-707.
- Quan Y.L. and Jerry M. H., 1997, Seismic attenuation tomography using the frequency shift method: *Geophysics*, **62**, 895-905.
- Parker, K., Lerner, R., and Waag, R., 1988, Comparison of techniques for in vivo attenuation measurements: *IEEE Trans. on Biomedical engineering*, **35**, 1064-1067.
- Pinnegar C R, Manisnha L., 2003, The S-transform with windows of arbitrary and varying shape: *Geophysics*, **68**, 381-385
- Portnoff M R., 1980, Time-frequency representation of digital signals and systems based on short-time Fourier analysis: *IEEE Trans. ASSP*, **28**, 111-116.
- Satish K.S., Partha S.R., Phil D.A. et al., 2003, Time-Frequency attribute of seismic data using continuous wavelet transform: 73rd Ann. Internat. Mtg., Soc. Expl. Geophys., Expanded Abstracts, 1481-1484.
- Strockwell R. G., Mansinha L., Lowe R. P., 1996, Localization of the Complex Spectrum, The S-Transform: *IEEE Trans. SP*, **44**, 998-1001.
- Varanini M., De P. G., Emdin M. et al., 1997, Spectral analysis of cardiovascular time series by the S-transform. *IEEE Comp.Cardiology*, **24**, 383-386.
- Wilson R., Calway A. D., and Pearson E.R.S., 1992, A generalized wavelet transform for Fourier analysis: the multiresolution Fourier transform and its application to image and audio signal analysis: *IEEE Trans.Info.Theory*, **38**, 674-690.
- Zhou W., Chen A.P., and Gu H. M., 2004, The application of combination time-frequency analysis in seismic prospecting: *Advance in Exploration Geophysics (China)*, **5**, 68-76.